Journal of Catalysis 288 (2012) 74–83

Contents lists available at SciVerse ScienceDirect

Journal of Catalysis

journal homepage: www.elsevier.com/locate/jcat

# Nickel-doped $Mn/TiO_2$ as an efficient catalyst for the low-temperature SCR of NO with $NH_3$: Catalytic evaluation and characterizations

Boningari Thirupathi, Panagiotis G. Smirniotis *

*Chemical Engineering Program, School of Energy, Environmental, Biological and Medicinal Engineering, University of Cincinnati, Cincinnati, OH 45221-0012, USA*

ARTICLE INFO

*Article history:*
Received 26 October 2011
Revised 4 January 2012
Accepted 9 January 2012
Available online 22 February 2012

*Keywords:*
Low-temperature $NH_3$-SCR
Manganese dioxide ($Mn^{4+}$)
Nickel oxide (NiO)
XPS
Hydrothermal stability
Nitric oxide

ABSTRACT

The $Mn/TiO_2$ and a series of $Mn–Ni/TiO_2$ catalysts were prepared by adopting incipient wetness technique and investigated for the low-temperature SCR of NO with $NH_3$ in the presence of excess oxygen. Our XPS results illustrated that the $MnO_2$ is the dominant phase with respect to the $Mn_2O_3$ phase ($Mn^{4+}/Mn^{3+}$ = 22.31, 96%), thus leading to a large number of $Mn^{4+}$ species ($Mn^{4+}$/Ti) over the titania support for the $Mn–Ni(0.4)/TiO_2$ catalyst. It is remarkable to note that the SCR performance of all the nickel-doped $Mn/TiO_2$ catalysts is accurately associated with the surface $Mn^{4+}$ concentrations. The co-doping of nickel into the $Mn/TiO_2$ with 0.4 Ni/Mn atomic ratio promotes the formation of surface $MnO_2$ phase and inhibits the formation of surface $Mn_2O_3$ sites. Our TPR results revealed that the addition of nickel oxide to titania-supported manganese results in the stabilization of the former in the form of $MnO_2$ rather than $Mn_2O_3$. Our TPR data results are in agreement with XPS results that the absence of the high-temperature (736 K) peak indicates that the dominant phase in the $Mn–Ni/TiO_2$ catalysts is $MnO_2$. The low-temperature reduction peak is shifted to much lower temperatures in nickel-doped $Mn/TiO_2$ catalysts. This increase in reducibility and the extremely dominant $MnO_2$ phase seem to be the reason for the high SCR activity of the $Mn–Ni/TiO_2$ catalysts.

Published by Elsevier Inc.

## 1. Introduction

The current technology for post-combustion removal of NO is the selective catalytic reduction (SCR) of NO by ammonia at medium to high temperatures. Industrially adopted catalysts for the practical applications of SCR reaction are $V_2O_5–MoO_3/TiO_2$ and $V_2O_5–WO_3/TiO_2$ [1,2]. However, the existing commercial catalytic system suffers from the drop of $N_2$ selectivity at high temperatures (573–673 K), the toxicity of vanadium pentoxide, high conversion of $SO_2$ to $SO_3$, and need to reheat the stack gas [3–6]. The development of low-temperature SCR catalysts working at 150–250 °C can offer a great solution to avoid all the problems associated with the existing commercial catalytic system.

The manganese oxide is well known for its high activity in the SCR of $NO_x$ at low temperatures [7–10]. In recent years, manganese-based catalysts attracted much attention due to their high activity for various reactions such as direct decomposition of nitric oxide [11], CO oxidation [12], $CH_4$ oxidation [13], and total oxidation of volatile organic compounds [14,15]. In all these reactions, the manganese oxide undergoes oxidation–reduction cycles (redox process). The $Mn^{4+}$ species and their redox process might be the reason for the high activity in the SCR reaction of NO with $NH_3$ at low temperatures. The manganese nitrate has been predominantly used in the preparation of the supported system in the SCR reaction of $NO_x$ studies, because of its high solubility in water and the ease of removal of the nitrate anion during calcination. The calcination temperature and metal loading have been found to determine the final oxidation state of the supported manganese oxide. On a support, $MnO_2$ is formed mainly below 700 K and $Mn_2O_3$ is formed at 900 K [16–18]. The supported $Mn_3O_4$ phase can be prepared by the slow reduction of $MnO_2$ at the temperature range of 665–700 K using hydrogen. Reduction at high temperatures in $H_2$ (900 K) is proposed to result in the formation of surface MnO at higher loadings [19].

The interaction of Mn with promoters or co-dopant species also influences its oxidation state [20]. For example, the co-doping of $Mn/TiO_2$ catalyst with copper cations formed mainly $Mn_2O_3$ phase at 723 K calcination temperature [21]. The interaction of Cr species with the $Mn/TiO_2$ catalyst produced surface $Mn^{3+}$ species at 923 K calcination temperature [22]. The contact of Ce with Mn by 0.8 M ratio creates surface $Mn_2O_3$, MnO, and $Mn_5O_8$ phases but not $MnO_2$ [23].

In the present work, we investigated whether phase change can occur with co-dopant nickel cations and promote the manganese phase transformation from $Mn_2O_3$ to $MnO_2$, thus increase in catalytic activity and stability of the catalyst. For this purpose, nickel metal was induced in the $Mn/TiO_2$ catalyst by varying the Ni/Mn

* Corresponding author. Fax: +1 513 556 3473.
*E-mail address:* panagiotis.smirniotis@uc.edu (P.G. Smirniotis).

0021-9517/$ - see front matter Published by Elsevier Inc.
doi:10.1016/j.jcat.2012.01.003

atomic ratio (Ni/Mn = 0, 0.2, 0.4, 0.6, and 0.8). However, the extremely dominant surface $MnO_2$ phase with respect to the $Mn_2O_3$ phase ($Mn^{4+}/Mn^{3+}$ = 22.31, 96%) was determined in our XPS analysis of the Mn–Ni(0.4)/$TiO_2$ catalyst. The high dispersion of surface $Mn^{4+}$ species on the $TiO_2$ support is achieved by the Mn–Ni/$TiO_2$ catalyst with Ni/Mn atomic ratio equal to 0.4. It is remarkable to note that the SCR performance of all the prepared catalysts is accurately correlated with the number of surface $Mn^{4+}$ species ($Mn^{4+}$/Ti ratio). The concentration and acidity (distribution) of Lewis acid sites on Mn/$TiO_2$ catalyst have significantly improved by the doping with Ni cations. The efficiency for NO removal, $N_2$ selectivity, temperature window, and time on stream stability (durability) enhanced greatly when Ni was substituted into the Mn/$TiO_2$ catalyst.

## 2. Experimental

### 2.1. Catalysts preparation

Mn/$TiO_2$ and a series of Mn–Ni/$TiO_2$ (Ni/Mn atomic ratio = 0.2, 0.4, 0.6, 0.8) catalysts were prepared by adopting a wet impregnation method. $TiO_2$ anatase (Hombikat UV 100 from Sachtleben Chemie) was used as support material to prepare these catalysts. Manganese nitrate ($Mn(NO_3)_2{\cdot}xH_2O$, 99.99%, Aldrich) and nickel nitrate ($Ni(NO_3)_2{\cdot}6H_2O$, Aldrich) were used as the source of manganese and nickel, respectively. The manganese loadings were selected as 5 wt.%, and the nickel loadings were varied ranging from 0 to 4 wt.%. The metal components of the catalysts are denoted as atomic ratios. All the ratios of the catalysts in this paper are Ni/Mn = 0, 0.2, 0.4, 0.6, 0.8. For convenience, we have given as Mn–Ni($x$)/$TiO_2$, where $x$ indicates the atomic ratio of nickel/manganese. To achieve this, the required quantities of precursors were added to a 100-mL beaker containing 2.0 g of support in 100 mL deionized water. The excess water was then slowly evaporated on a water bath with continuous stirring at 70 °C. For comparison purposes, $TiO_2$ anatase (Hombikat) support alone was mixed in deionized water and then water was evaporated with continuous heating and stirring. The resulting materials were oven-dried at 120 °C for 12 h and were ground and sieved (80–120 mesh) to obtain homogeneous powder. Prior to the reaction studies, the powder was calcined in a tubular oven at 400 °C for 2 h under continuous air flow (150 mL $min^{-1}$).

### 2.2. X-ray diffraction

The powder XRD patterns were recorded on a Phillips Xpert diffractometer using nickel-filtered Cu Kα (wavelength 0.154056 nm) radiation source and a scintillation counter detector. An aluminum holder was used to support the catalyst samples. The intensity data were collected over a 2$\theta$ range of 10–80° with a step size of 0.025° and a step time of 0.25 s. Crystalline phases were identified by comparison with the reference data from International Center for Diffraction Data (ICDD) files.

### 2.3. BET surface area and pore volume measurements

$N_2$ adsorption–desorption isotherms were obtained at liquid nitrogen temperature (77 K) using Micromeretics Gemini surface area apparatus. Prior to $N_2$ adsorption, 0.08–0.1 g of the samples were degassed under helium atmosphere at 200 °C for 2 h in the degassing port of the instrument. The adsorption isotherms of nitrogen were collected by using approximately six values or relative pressure ranging from 0.05 to 0.99 and by taking 0.162 $nm^2$ as the molecular area of the nitrogen molecule.

### 2.4. Temperature-programmed reduction ($H_2$-TPR)

Hydrogen temperature-programmed reduction ($H_2$-TPR) of various catalyst samples was performed by means of an automated catalyst characterization system (Micromeritics, model AutoChem II 2910), which incorporates a thermal conductivity detector (TCD). The experiments were carried out at a heating rate of 5 °C/min. The reactive gas composition was 10% $H_2$ in argon with a flow rate of 20 mL $min^{-1}$ (STP). The amount of $H_2$ consumed by the catalyst sample in a given temperature range (in mmol $g^{-1}$) was calculated by the integration of the corresponding TCD signal intensities. Prior to the analysis, approximately 50 mg of the catalysts were pretreated at 200 °C for 2 h in ultra-high-pure helium (30 mL $min^{-1}$) stream after preheating samples were tested by increasing the temperature from 50 to 800 °C. The temperature was then kept constant at 800 °C until the signal of hydrogen consumption returned to the initial values. The TPR runs were carried out with a linear heating rate (10 °C/min) in a flow of 4% $H_2$ in argon with a flow rate of 20 mL $min^{-1}$. The hydrogen consumption was measured quantitatively by a thermal conductivity detector. A mixture of isopropanol and liquid nitrogen was used in the trapper to collect the formed water during the TPR experiment.

### 2.5. Oxygen pulse chemisorptions

The site time yield (STY), oxygen uptake, and the active metal dispersion on the surface of the titania support were determined by oxygen chemisorption measurements. These measurements were obtained in a pulse (Micromeretics Autochemi I 2910 system) mode using He as carrier gas (30 STP $cm^3$ $min^{-1}$). Prior to the analysis, approximately 0.050 g of catalyst samples were reduced in flowing $H_2$ (50 STP $cm^3$ $min^{-1}$) at 250 °C for 2 h and then flushed at the same temperature for 30 min in the He carrier flow [10]. Then, oxygen pulses (1 mL loop volume) were injected onto the carrier gas until saturation of the sample was attained. The oxygen uptake was quantified by a TCD connected to a 2910 Autochem I (Micromeretics instrument).

### 2.6. $NH_3$-TPD

$NH_3$-TPD data were collected on a Micromeritics Autochem 2910 Automated Catalyst Characterization System. Each sample (ca. 100 mg of finely ground powder) was initially pretreated through heating at 200 °C in an ultra-high-pure He stream (30 mL/min) with a 2 h hold. After that, the furnace temperature was lowered to 100 °C, and the samples were then saturated with anhydrous $NH_3$ (4% in He) at a flow rate of 30 mL/min for 1 h. The sample was flushed with 30 mL/min of He for 2 h to remove weakly bound (physisorbed) $NH_3$, after which the sample temperature was reduced to 50 °C. Once a stable baseline by thermal conductivity detector had been achieved, the temperature was then ramped from 50 °C at a rate of 5 °C/min to 800 °C.

### 2.7. In situ FT-IR spectroscopy

FT-IR spectra were recorded using a Bio-Rad (FTS-40). The scans were collected at a scan speed of 5 kHz, resolution of 2.0, and an aperture opening of 2.0 $cm^{-1}$. Sixteen scans were averaged for each normalized spectrum. Circular self-supporting thin wafers (8 mm diameter) consisting of 12 mg of material were used for the study. The wafers were placed in a high-temperature cell with $CaF_2$ windows and purged *in situ* in the IR cell with prepurified-grade helium (30 mL $min^{-1}$, Wright Brothers) at 473 K for 2 h to remove any adsorbed impurities. After this step, the samples were cooled to 323 K and $NH_3$ (3.9 vol.% in He) was introduced into the cell with a flow of 30 mL $min^{-1}$ for 1 h at 323 K to ensure complete satura-

tion of the sample. Physisorbed ammonia was removed by flushing the wafer with helium for sufficient time (3 h) at 373 K. Subsequently, the *in situ* FT-IR spectra were recorded by the evacuation of ammonia at successive temperatures 323, 373, 423, 473, and 523 K.

### 2.8. X-ray photoelectron spectroscopy (XPS)

The X-ray photoelectron spectroscopy (XPS) experiments were carried out on a Pyris-VG thermo scientific X-ray photoelectron spectrometer system equipped with a monochromatic Al Kα (1486.7 eV) as a radiation source at 300 W under UHV ($6.7 \times 10^{-8}$ Pa). Sample charging during the measurement was compensated by an electron flood gun. The electron takeoff angle was 45° with respect to the sample surface. The spectra were recorded in the fixed analyzer transmission mode with pass energies of 89.45 and 35.75 eV for recording survey and high-resolution spectra, respectively. The powdered catalysts were mounted onto the sample holder and evacuated overnight at room temperature at a pressure on the order of $10^{-7}$ torr. Binding energies (BE) were measured for C 1s, O 1s, Ti 2p, Mn 2p, and Ni 2p. A recorded Auger spectrum for Mn was very weak. Sample charging effects were eliminated by correcting the observed spectra with the C 1s binding energy (BE) value of 284.6 eV. An estimated error of ±0.1 eV can be considered for all the measurements. The overlapped Mn 2*p* peaks were deconvoluted into several sub-bands by searching for the optimal combination of Gaussian bands with the correlation coefficients ($r^2$) above 0.99. The Mn 2*p* peak was deconvoluted using the Gaussian function.

### 2.9. Apparatus and catalytic experiments

The low-temperature reduction of NO by ammonia ($NH_3$-SCR) with excess oxygen activity measurements were carried out at atmospheric pressure in a fixed-bed continuous flow quartz reactor with an internal diameter of 6 mm. 0.1 g of catalyst (80–120 mesh) was placed in the reactor in between two glass wool plugs, otherwise mentioned. All the gas flows were measured and calibrated using a digital flow meter (Humonics Hewlett Packard Optiflow 520). The reaction gas mixture normally consisted of 400 ppm NO, 400 ppm $NH_3$, 2 vol.% $O_2$, and He in balance.

$$4NO + 4NH_3 + O_2 = 4N_2 + 6H_2O \quad (1)$$

A total of 10 vol.% $H_2O$ vapor was used for the hydrothermal stability test. The premixed gases oxygen (4% in He, Wright Brothers), ammonia (3.99% in He, Wright Brothers), and nitric oxide (2.0% in He, Matheson) were used as received. ISCO series D pump controller was used to feed the 10 vol.% concentration of water vapor. The tubing of the reactor system was heat-traced to prevent the formation and deposition of ammonium sulfate/bisulfate and ammonium nitrate. The NO and $NO_2$ concentrations were continually monitored by a chemiluminescence NO/$NO_x$ detector (Eco Physics CLD 70S). To avoid errors caused by the oxidation of ammonia in the converter of the NO/$NO_x$ analyzer, an ammonia trap containing phosphoric acid solution was installed before the sample inlet to the chemiluminescence detector [3]. The reactor was heated externally via a tubular furnace regulated by a temperature controller (Omega CN 2041), with a thermocouple inserted into the catalyst bed. Prior to the catalytic experiments, the catalyst was activated *in situ* by passing oxygen (4% in He, Wright Brothers) for 2 h at 200 °C temperature. The reactants and products were analyzed *online* using a Quadrapole mass spectrometer (MKS PPT-RGA) and a chemiluminescence detector (Eco Physics CLD 70S). Reactant and product contents in the reactor effluent were recorded only after steady state was achieved at each temperature step. The $N_2$ selectivity and NO conversions were calculated as in our previous papers [7–10].

## 3. Results and discussion

Initially, we evaluated the potential catalytic performance of all the prepared catalysts ($Mn/TiO_2$ and $Mn–Ni/TiO_2$ with Ni/Mn atomic ratio = 0.0, 0.2, 0.4, 0.6, 0.8) at 200 °C to optimize the Ni content and to ensure the influence of $Ni^{2+}$ co-cations on NO conversion. From our results, one can observe that the partial loading of Mn with Ni elements could indeed influence the SCR activity of $Mn/TiO_2$ catalyst. The catalytic performance results for the SCR of NO with ammonia over titania-supported manganese as well as manganese–nickel catalysts are tested at GHSV 50,000 $h^{-1}$ in the presence of 2 vol.% of oxygen (Fig. 1). The nickel loading has a strong influence on the conversion and $N_2$ selectivity, since nickel loading with the Ni/Mn ratio = 0.4 catalyst exhibits a maximum conversion of 100% with huge $N_2$ selectivity at 200 °C (Fig. 1). This would indicate that an optimal dispersion of Mn–Ni species on the support surface is attained with this amount of nickel in the $Mn–Ni/TiO_2$ catalyst. The $Mn/TiO_2$ catalyst does not accomplish high NO conversions at 200 °C. As the Ni/Mn atomic ratio increases up to 0.4 on the $TiO_2$-supported manganese surface, the NO conversion increased monotonically and then decline for higher loadings (Ni/Mn = 0.6, 0.8) of nickel. As can be noted from the Fig. 1, high conversion of NO (100%), $N_2$ selectivity achieved over the $Mn–Ni(0.4)/TiO_2$ catalyst. The $Mn–Ni(0.4)/TiO_2$ afforded highly remarkable catalytic activity and $N_2$ selectivity relative to the other catalysts tested with GHSV 50,000 $h^{-1}$ at 200 °C temperature.

With these interesting results in hand, we evaluated the SCR activity of all the prepared catalysts to ensure about the temperature window and the influence of nickel content on the SCR activity at the temperature range of 160–240 °C (Fig. 2). Under identical operating conditions, the pure $Mn/TiO_2$ catalyst demonstrated poor catalytic performance at below 200 °C and it is evident that the NO conversions drastically decline with time at above 200 °C. This is probably due to the sintering of manganese species over the surface of titania support at high temperatures. The undoped $Mn/TiO_2$ showed very narrow operation temperature window for the $NH_3$-SCR reaction, and the maximum NO conversions could not reach 100%. Eventually, the addition of nickel species to the $Mn/TiO_2$ catalyst (Ni/Mn ratio = 0.4) broadened the temperature window and demonstrated complete NO conversion at the temperature range of 200–250 °C. The doping of nickel co-cations with 0.4

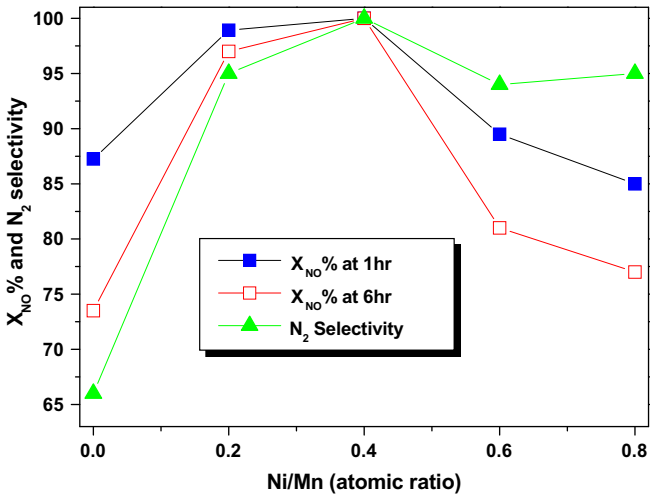


**Fig. 1.** Effect on NO conversion and $N_2$ selectivity in the SCR reaction of $Mn/TiO_2$ and $Mn–Ni/TiO_2$ catalysts with respect to the Ni/Mn atomic ratio; temperature = 200 °C; GHSV = 50,000 $h^{-1}$; feed: NO = 400 ppm, $NH_3$ = 400 ppm, $O_2$ = 2 vol.%, He carrier gas, catalyst = 0.1 g, total flow = 140 mL $min^{-1}$. $N_2$ selectivities at 6 h of reaction.

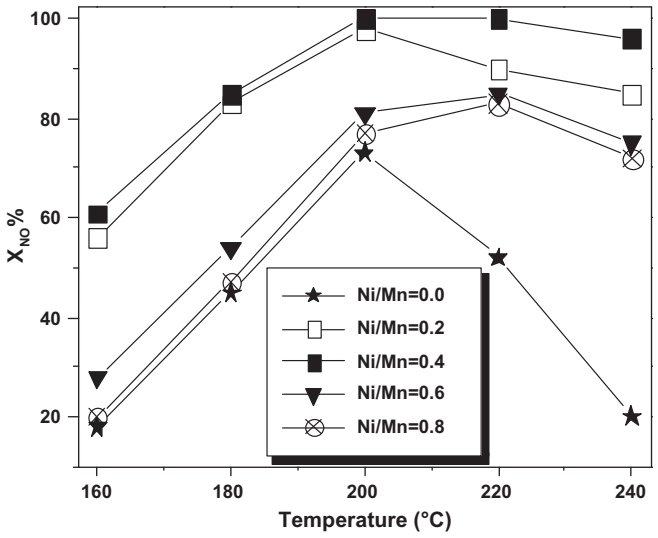


**Fig. 2.** Influence of Ni/Mn atomic ratio on NO conversion in the SCR reaction at a temperature range (160–240 °C) over Mn–Ni/$TiO_2$ catalysts; GHSV = 50,000 $h^{-1}$; feed: NO = 400 ppm, $NH_3$ = 400 ppm, $O_2$ = 2 vol.%, He carrier gas, catalyst = 0.1 g, total flow = 140 mL $min^{-1}$. $X_{NO}$% = conversion of NO at 6 h on stream.

Ni/Mn atomic ratio greatly improved the thermal stability of the $Mn/TiO_2$ catalyst since the Mn–Ni(0.4)/$TiO_2$ demonstrated steady high NO conversions at 300 °C (not shown). At the reaction temperature 200 °C, further increase in the nickel content exceeding that of 0.4 Ni/Mn atomic ratio decreased the SCR activity of the catalyst. This is due to the interaction between the $TiO_2$ and manganese–nickel oxide which becomes feeble, and the number of participating surface manganese oxide sites decrease with the increase in nickel loading. This occurrence was also proved by our XPS analysis as we will demonstrate below. The $NH_3$-SCR activity, $N_2$ selectivity, stability, and operation temperature window of the $Mn/TiO_2$ catalyst improved greatly by the addition of optimal nickel content (Ni/Mn atomic ratio = 0.4).

Subsequently, the time on stream patterns of all the prepared catalysts were evaluated at 200 °C, to check the impact of Ni species in time stability of the $Mn/TiO_2$ catalyst (Fig. 3). Among all the catalysts, undoped $Mn/TiO_2$ (Ni/Mn = 0.0) showed poor stability since the catalytic activity monotonically dropped in six hours of continuous stream. It is apparent that the addition of nickel to the $Mn/TiO_2$ catalyst has enhanced the stability of the catalyst. In particular, Mn–Ni(0.4)/$TiO_2$ catalyst showed a remarkable performance by exhibiting 100% NO conversion even after 240 h on stream. The Mn–Ni(0.6)/$TiO_2$ and Mn–Ni(0.8)/$TiO_2$ catalysts were rapidly deactivating with time. These results demonstrate that the time on stream performance of the catalysts decreased in the following order: Mn–Ni(0.4)/$TiO_2$ ≫ Mn–Ni(0.2)/$TiO_2$ ⋙ Mn–Ni(0.6)/$TiO_2$ > Mn–Ni(0.8)/$TiO_2$ > $Mn/TiO_2$.

It is also important to evaluate the durability of SCR catalysts in the presence of $H_2O$ vapors in the feed. Fig. 4 illustrates the tolerance of Mn–Ni(0.4)/$TiO_2$ catalyst to steam poisoning for 240 h during the SCR of NO with $NH_3$ at low temperatures. Several reported catalysts for the low-temperature SCR of NO with $NH_3$ have the problem of deactivation when water vapor was introduced into the stream [24–26]. We carried out the SCR of NO reaction with high gas hourly space velocity (GHSV) 50,000 $h^{-1}$ in the presence of 10 vol.% $H_2O$ vapors in the feed (Fig. 4) to test the durability of the catalyst.

Initially, our best catalyst Mn–Ni(0.4)/$TiO_2$ showed high NO conversion in the absence of $H_2O$ (10 vol.%), a steady-state NO conversion of 100% with $N_2$ selectivity at 200 °C is obtained within the first 6 h. In the present study, the Mn–Ni(0.4)/$TiO_2$ catalyst showed an extraordinary performance ($X_{NO}$% = 100%) even in the presence of 10 vol.% water vapor inlet concentrations. The bimetallic combination of Mn and Ni with 0.4 Ni/Mn atomic ratio produced very stable and durable catalyst that did not deactivate for the tested period. The $N_2$ selectivity Mn–Ni(0.4)/$TiO_2$ catalyst remained at 100% after 240 h on stream. These results clearly suggest that the Mn–Ni(0.4)/$TiO_2$ displays a satisfactory extent of stability and durability properties. The system is successful because of its high activity and resistance to steam poisoning. The addition of $H_2O$ (10 vol.%) in the feed gas does not seem to create an eternal alteration to the surface manganese species, most probably due to the existence of high redox potential pairs of Mn and Ni in the structure, permitting an efficient active catalyst.

To gain additional insight into the active surface manganese species for the low-temperature SCR reaction, the $H_2$ temperature-programmed reduction of the pure manganese oxide (from $Mn(NO_3)_2{\cdot}xH_2O$, 99.99% metals basis) was carried out and evaluated for the SCR reaction. The reduction profile of unsupported manganese oxide was characterized by three different reduction peaks at 640, 728, and 790 K (Fig. 5). A low-temperature reduction

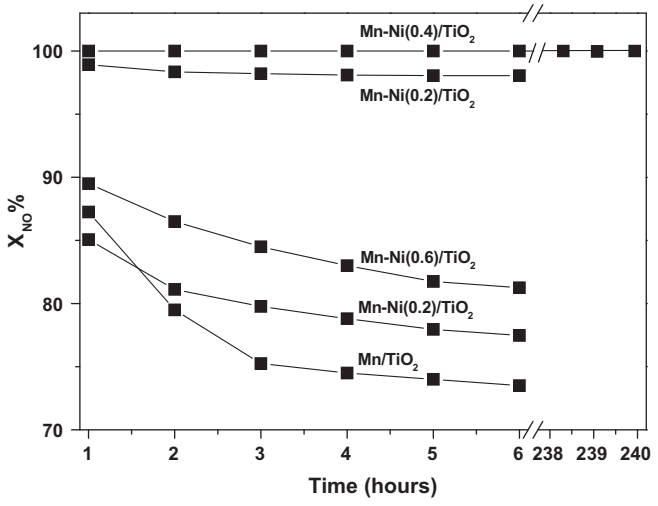


**Fig. 3.** SCR of NO with $NH_3$ at 200 °C temperature over $Mn/TiO_2$ and Mn–Ni/$TiO_2$ catalysts; (■): GHSV = 50,000 $h^{-1}$; feed: NO = 400 ppm, $NH_3$ = 400 ppm, $O_2$ = 2 vol.%, He carrier gas, total flow = 140 mL $min^{-1}$, $X_{NO}$% = conversion of NO; catalyst = 0.1 g.

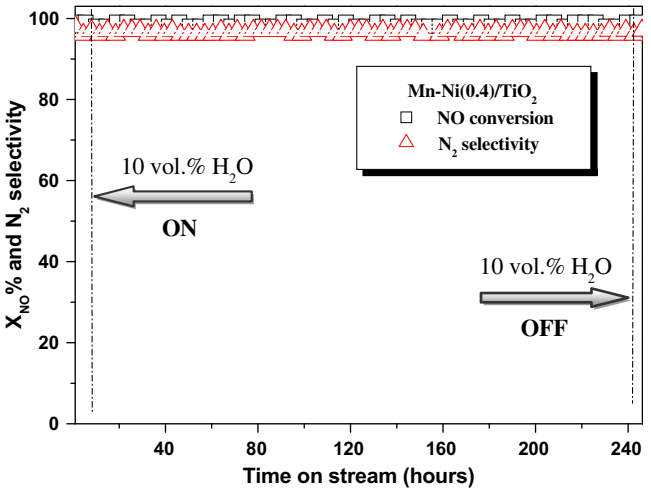


**Fig. 4.** Influence of inlet water concentrations (10 vol.%) on NO conversion in the SCR reaction over Mn–Ni(0.4)/$TiO_2$ catalyst at 200 °C; feed: NO. 400 ppm $NH_3$/NO. 1.0, $O_2$. 2 vol.%, He carrier gas, catalyst. 0.1 g, GHSV. 50,000 $h^{-1}$.

peak ($T_1$) is observed at 640 K, which corresponds to the reduction of $MnO_2$ to $Mn_2O_3$. The subsequent reduction peak at 728 ($T_2$) is attributed to the reduction of $Mn_2O_3$ to $Mn_3O_4$. A high-temperature peak maxima at 790 K ($T_3$) can be interpreted as a reduction of $Mn_3O_4$ to MnO [27]. Usually, the manganese (II) oxide (MnO) is a green crystalline solid with $FM\bar{3}m$ space group [28], it is interesting to note that the manganese (IV) oxide sample turned into a green crystalline solid after the treatment for the sample with $H_2$ at 1083 K (during $H_2$-TPR experiment). It can be concluded from this observation that the sample finally converts into MnO but not into metallic manganese ($Mn^0$). From our $H_2$-TPR results, it is evident that the unsupported manganese (IV) oxide sample undergoes stepwise reduction of $MnO_2$ to $Mn_2O_3$, $Mn_2O_3$ to $Mn_3O_4$, and $Mn_3O_4$ to MnO. Subsequently, the catalytic reduction of NO over the pure manganese oxides with respect to the temperature was investigated to understand the active phase of manganese for the SCR of NO at low temperatures (Fig. 6). To avoid the phase transformations, all the manganese oxides were prepared by *in situ* method. Prior to the catalytic experiments of pure $Mn_xO_y$ phases, the manganese oxides ($MnO_2$, $Mn_2O_3$, $Mn_3O_4$, MnO) were synthesized *in situ* by passing hydrogen through a fixed-bed quartz reactor at carefully selected temperatures.

Prior to the catalytic performance tests of pure Mn oxides, a reaction with undoped Hombikat $TiO_2$ (calcined at 400 °C) was performed at 200 °C to observe the catalytic activity of the $TiO_2$ support and the efficiency of our SCR unit. As estimated, the NO and $NH_3$ conversions were zero when only $TiO_2$ anatase (Hombikat) was used as catalyst at relevant conditions (not shown in figure). The evaluation of the catalyst activity of pure Mn oxides for the SCR of NO with ammonia at the temperature range 393–513 K is tested in the presence of 2 vol.% of oxygen (Fig. 6). It should be noted that a relatively low gas hourly space velocity was used for this set of experiments in order to allow us to get significant level of NO conversion of the pure Mn oxides. All these reactions were performed in a quartz fixed-bed continuous flow reactor (i.d. 6 mm, 51 cm) at atmospheric pressure. The typical reactant gas composition was as follows: 400 ppm NO, 400 ppm $NH_3$, 2% $O_2$, and balance helium. Prior to the each reaction, unsupported manganese oxides of different oxidation state were prepared *in situ* and evaluated for the SCR of NO with ammonia between 393 and 513 K. These normalized results demonstrate the nitric oxide reduction performance of the pure Mn oxides decreased in the following order: $MnO_2 \gg Mn_2O_3 \lll Mn_3O_4 \cong MnO$. The nitric oxide reduction results of MnO have not been incorporated in Fig. 6, since it had been progressively converted into

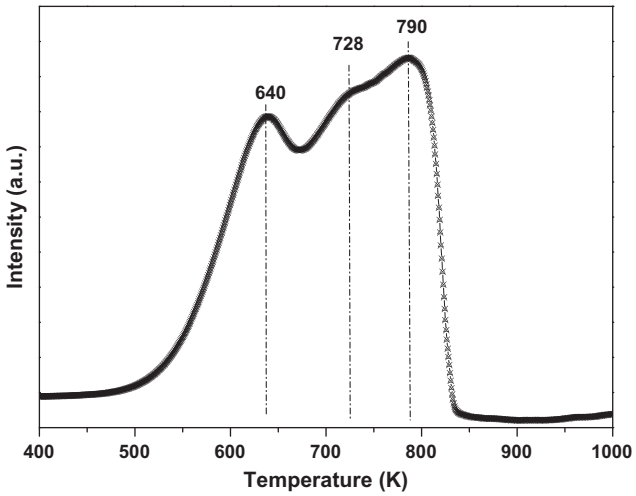


**Fig. 5.** The reduction profile ($H_2$-TPR) of unsupported manganese oxide.

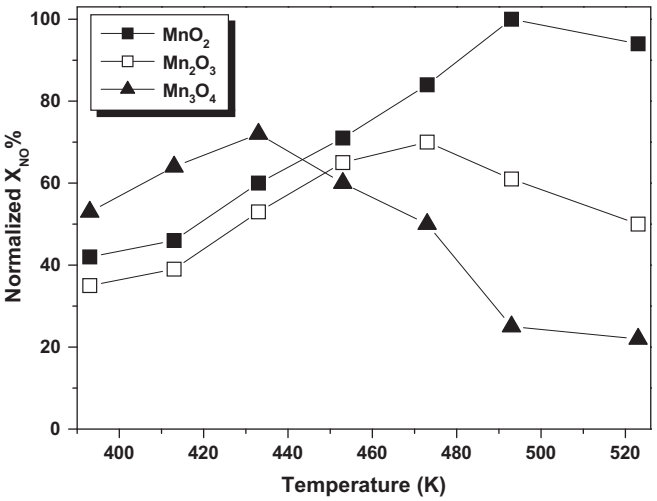


**Fig. 6.** Influence of Mn oxidation state on NO conversion in the SCR reaction of NO with respect to temperature: GHSV = 8000 $h^{-1}$; feed: NO = 400 ppm, $NH_3$ = 400 ppm, $O_2$ = 2 vol.%, He carrier gas.

$Mn_3O_4$ during the SCR experiment. For this reason only, the MnO also showed similar results as the $Mn_3O_4$ in the SCR of NO reaction. All the above results clearly suggest that the oxidation state of the surface Mn is decisive and the surface $Mn^{4+}$ species are highly active for the SCR of NO reaction with ammonia at low temperatures.

In order to obtain the information about the oxidation state of manganese and nickel cations on the catalyst surface (which was invisible under XRD) and to ensure the chemical compositions (atomic concentrations) of the surface layer, XPS spectra of the samples were recorded. The $MnO_2$ and $Mn_2O_3$ were prepared using aqueous solutions of manganese nitrates [29], and $Mn_3O_4$ was prepared by the slow reduction of $MnO_2$ at 473 K in $H_2$ [30]. The pure MnO was prepared by the slow reduction of $MnO_2$ at 900 K in $H_2$. The above prepared samples were used for the reference manganese phase compounds. However, our XPS spectra of the reference samples of $MnO_2$, $Mn_2O_3$, $Mn_3O_4$, and MnO exhibited the Mn $2p_{3/2}$ peak at around 642.3, 641.3, 641.4, and 641.5 eV, respectively (Table 1). Two main peaks due to Mn $2p_{3/2}$ and Mn $2p_{1/2}$ of the Mn/$TiO_2$ and nickel-doped Mn/$TiO_2$ samples are shown in Fig. 7. It has been well established that the $Mn^{4+}$ peak, $Mn^{3+}$ peak, and Mn nitrate peaks appear at 642.1 ± 0.2 eV, 641.3 ± 0.2 eV, and 644.2 ± 0.4 eV, respectively [8,31,22]. For the identification of the surface manganese oxide phases and the relative percentages of $Mn^{4+}$, $Mn^{3+}$, $Mn^{n+}$ species, the overlapped Mn 2*p* peaks were deconvoluted into several peaks by searching for the optimal combination of Gaussian bands with the correlation coefficients ($r^2$) above 0.99 (PeakFit, Version 4.0.6, AISN Software Inc.). The deconvoluted peaks are signed as specific phases of manganese ($MnO_2$, $Mn_2O_3$, Mn nitrate) in each spectrum (Fig. 7). The relative percentages of manganese, nickel, and titania species were calculated by the area ratio of the corresponding characteristic peaks. The results are listed in Table 1.

As shown in Fig. 7 and Table 1, the manganese species ($Mn^{4+}$, $Mn^{3+}$) can be characterized by Mn $2p_{3/2}$ and Mn $2p_{1/2}$ peaks located between 639.0 eV and 658 eV. It has been found in our studies and established in the literature that the $2p_{3/2}$ binding energy of $Mn^{4+}$ ($MnO_2$) is 642.1 ± 1 eV, while the corresponding $Mn^{3+}$ ($Mn_2O_3$) has a binding energy at 641.3 ± 1 eV [8,31,22,32,33]. In all cases, the as-prepared catalyst surfaces were Mn enriched, as depicted by the consistently higher value of Mn/Ti surface relative to Ni/Ti. More specifically, in Mn–Ni(0.4)/$TiO_2$, $Mn^{4+}$ species are most enriched on the $TiO_2$ surface with higher surface $MnO_2$ phase relative to that of other catalysts.

**Table 1**
Binding energy, surface atomic ratio of $Mn^{4+}/Mn^{3+}$, Ni/Mn, and $Mn^{4+}/Ti$ for the prepared catalysts determined from deconvoluted XPS spectra.

| Catalyst | B.E. (eV) | | | M′ | | | | $(Mn^{4+}/Mn^{3+})$[a] | $(Mn^{4+}/Mn^{n+})$[a] | Ni/Mn [a] | $Mn^{4+}/Ti$ [a] |
|---|---|---|---|---|---|---|---|---|---|---|---|
| | Ti $2p_{3/2}$ | Ti $2p_{1/2}$ | O 1s | Mn $2p_{3/2}$ | Mn $2p_{1/2}$ | Ni $2p_{3/2}$ | Ni $2p_{1/2}$ | | | | |
| $MnO_2$ | – | – | – | 642.1 | 653.6 | – | – | – | – | – | – |
| $Mn_2O_3$ | – | – | – | 641.3 | 653.0 | – | – | – | – | – | – |
| $Mn_3O_4$ | – | – | – | 641.4 | 652.9 | – | – | – | – | – | – |
| MnO | – | – | – | 641.5 | 653.1 | – | – | – | – | – | – |
| 5 $Mn/TiO_2$ | 458.6 | 464.3 | 529.9 | 642.1 | 653.6 | – | – | 02.02 | 0.58 | – | 0.020 |
| | | | | 641.3 | 653.0 | | | | | | |
| $Mn–Ni(0.2)/TiO_2$ | 458.6 | 464.1 | 530.1 | 642.1 | 653.6 | $2p_{3/2}$ | $2p_{1/2}$ | 04.88 | 1.18 | 0.17 | 0.069 |
| | | | | 641.3 | 653.0 | 855.8 | 869.5 | | | | |
| $Mn–Ni(0.4)/TiO_2$ | 459.1 | 464.6 | 530.3 | 642.1 | 653.6 | $2p_{3/2}$ | $2p_{1/2}$ | 22.31 | 1.33 | 0.43 | 0.073 |
| | | | | 641.3 | 653.0 | 856.3 | 874.6 | | | | |
| $Mn–Ni(0.6)/TiO_2$ | 458.8 | 464.5 | 530.0 | 642.1 | 653.6 | $2p_{3/2}$ | $2p_{1/2}$ | 01.82 | 0.63 | 0.67 | 0.053 |
| | | | | 641.3 | 653.0 | 856.1 | 873.8 | | | | |
| $Mn–Ni(0.8)/TiO_2$ | 459.0 | 464.6 | 530.3 | 642.1 | 653.6 | $2p_{3/2}$ | $2p_{1/2}$ | 01.44 | 0.51 | 0.80 | 0.049 |
| | | | | 641.3 | 653.0 | 856.2 | 874.1 | | | | |

[a] Relative amounts are according to the metal atomic ratio.

Table 1 shows the atom percentage of catalysts determined by XPS. The relative atomic percentage value of $Mn^{4+}/Mn^{3+}$ characterized by XPS was significantly high for the $Mn–Ni(0.4)/TiO_2$ catalyst ($Mn^{4+}/Mn^{3+}$ = 22.31, 96%), whereas $Mn_2O_3$ phase is in contest with $MnO_2$ in other catalysts ($Mn^{4+}/Mn^{3+}$ = 1.34–12.67) (Table 1, Fig. 7). The formation of surface $MnO_2$ phase is improved a lot by the co-doping of nickel into the $Mn/TiO_2$ with 0.4 Ni/Mn atomic ratio. Among all the catalysts, high surface $Mn^{4+}$ concentrations ($Mn^{4+}$/Ti) were observed for the $Mn–Ni(0.4)/TiO_2$ catalyst. This is due to the higher surface coverage by manganese (IV) oxide and/or its higher dispersion on the $TiO_2$ support. It is interesting to note that the SCR performance of all the prepared catalysts (Fig. 1) is accurately correlated with the surface $Mn^{4+}$ concentrations (Fig. 8). The $Mn_xO_y$ catalytic activity has been ascribed to the potential of Mn to form several oxides and to provide oxygen selectively from its crystalline lattice. Since its labile oxidation state, Mn is acting as an active component in the redox process.

Conversely, the amount of $Mn_xO_y$ needed to cover the support surface as a monomolecular layer can be estimated from structural calculations [34]. The monolayer surface coverage is defined as the maximum amount of $Mn_xO_y$ in contact with the metal oxide support. From the M–O bond lengths of the crystalline $Mn_2O_3$, monolayer surface coverage is estimated to be 0.05 wt.% Mn per $m^2$ of the support [26]. Very interestingly, our best catalyst Mn–$Ni(0.4)/TiO_2$ composition is equivalent to near or just below the monolayer capacity of surface manganese on the $TiO_2$ support. This is probably due to the involvement of Ni species with $Mn_xO_y$ dispersion over the titania anatase support. Our previous XRD studies clearly indicate that the formation of bulk manganese oxide commences from the 8–9 wt.% of manganese over the titania support [10]. The high dispersion of $Mn^{4+}$ species monolayer on the $TiO_2$ support is achieved by a total 7 wt.% of $Mn–Ni/TiO_2$ with Ni/Mn atomic ratio equal to 0.4. Moreover, the Mn–Ni loadings are nearly equivalent to the theoretical monolayer capacity. As can be seen from the Fig. 8, the existence of the number of surface $Mn^{4+}$ species over the $TiO_2$ support ($Mn^{4+}/TiO_2$) is directly related to the potential activity of the particular catalyst. In other words, a high concentration of surface $Mn^{4+}$ species equivalent to the monolayer capacity on the support surface is highly essential for obtaining better yields. These studies are in good agreement with our activity studies of pure manganese oxides. Kapteijn et al. [27] also investigated for the active phase of manganese toward the SCR of NO at low temperatures (Fig. 6) and found that the $MnO_2$ is the preeminent phase for the SCR reaction. The $MnO_2$ showed an excellent catalytic performance, this is probably due to the poor crystalline structure of manganese oxide material and defective structural composition [35]. In addition, the presence of other transition metal cations could also favor the existence surface manganese ($Mn^{4+}$) species over the support [36].

The highly dispersed manganese and nickel species over the surface of titania anatase is ascertained by the XRD. Interestingly, our XRD studies revealed that the promoter oxide (NiO) does not favor any titania phase transformation. Powder X-ray diffraction patterns of the various nickel-doped titania-supported manganese catalysts calcined at 673 K for 2 h are shown in Fig. 9. For pure $TiO_2$ sample, the strong characteristic peaks of titania anatase can be observed. All the samples with various Ni/Mn atomic ratio showed broad diffraction lines typically at $d$ = 3.54, 1.90, and 2.40 Å, which corresponds to anatase phase (JCPDS #71-1169 and 21-1272). For all the prepared catalysts, X-ray reflections at $d$ = 2.41, 1.63, and 2.11 Å are not found, which are corresponding to $MnO_2$ phase (JCPDS #04-0779). These results are suggesting that the manganese oxide is in a highly dispersed state or the crystallites formed are less than 5 nm, and also insertion of manganese ions into the titania lattice [37]. Our XPS studies on surface atomic ratio of Mn/Ti would explain that the manganese is intercalated in the $TiO_2$ (Hombikat) lattice structure at lower loadings due to the high surface and the smaller particle size of the support. Due to this reason, thought that the Mn is highly dispersed at a certain level called two-dimensional monolayer coverage. This highly dispersed manganese or poor crystalline structure of manganese oxide has been suggested to improve the existence of oxygen vacancies and perform a best catalytic performance [7]. It was proposed that a small amount of co-doping metal prevents manganese oxide reaching a crystalline structure [38,39].

The BET surface area, average pore diameter, and pore volume of the titania (anatase), $Mn/TiO_2$, $Mn–Ni/TiO_2$ (Ni/Mn = 0.2, 0.4, 0.6, 0.8) catalysts are summarized in Table 2. The specific surface area of the pure titania catalyst dropped to 161 $m^2\,g^{-1}$. It can be explained that the crystallinity and particle size of the support material increased after calcination at 400 °C. By increasing the Ni/Mn atomic ratio from zero to 0.4, we observe a monotonic increase in the surface area and pore volume. However, the BET surface area and pore volume decrease gradually with the increase in nickel content (Ni/Mn = 0.6, 0.8), which may be caused by the blocking effect of the support pores by the loading of nickel oxide. However, the co-doping of nickel cations onto the $Mn/TiO_2$ has apparently enhanced the specific surface area of the catalyst. Among all the catalysts, $Mn–Ni(0.4)/TiO_2$ catalyst attained the high surface area (200 $m^2/g$) and high pore volume (0.42 $cm^3/g$). It is due to high dispersion of manganese and nickel oxides over the titania support. In order to investigate the synergistic promoting

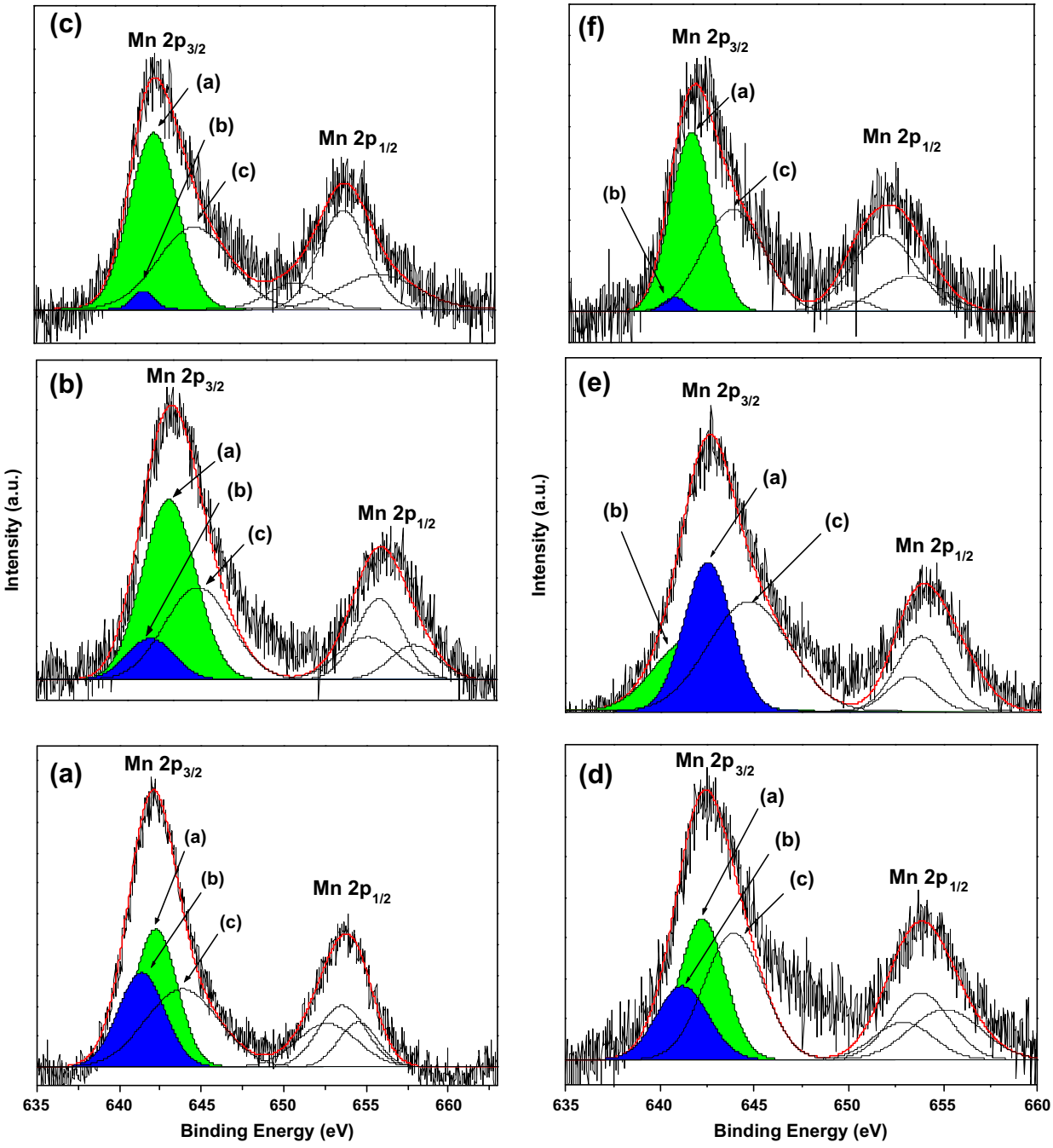


**Fig. 7.** Deconvoluted Mn 2*p* (XPS) spectra of (a) $MnO_x/TiO_2$ (b) Mn–Ni(0.2)/$TiO_2$, (c) Mn–Ni(0.4)/$TiO_2$, (d) Mn–Ni(0.6)/$TiO_2$, (e) Mn–Ni(0.8)/$TiO_2$, (f) spent Mn–Ni(0.4)/$TiO_2$ catalysts.

effect of Ni species in Mn–Ni/$TiO_2$ catalyst, we normalized the NO conversion over the catalysts with different Ni/Mn atomic ratios using BET surface area (Fig. 10). With the increase in Ni/Mn atomic ratio equal to 0.4, the normalized NO conversion showed a monotonic enhancement. Further increase in Ni/Mn atomic ratio decreased the normalized NO conversion, indicating that the Mn/$TiO_2$ catalyst is promoted by the optimized amount of Ni species, and Mn species are the main active components. Though the normalized $NH_3$-SCR activity of Mn–Ni(0.2)/$TiO_2$ catalyst is equivalent to the Mn–Ni(0.4)/$TiO_2$ at 200 °C, from the viewpoint of reaction temperature broadening application, we chose Mn–Ni(0.4)/$TiO_2$ as the model catalyst for further study due to its high apparent $NH_3$-SCR activity at low temperatures. However, the normalized NO conversion of Mn–Ni(0.2)/$TiO_2$ decreased at 240 °C.

The Mn/$TiO_2$ sample prepared by incipient wetness technique shows TPR patterns characterized by three narrow peaks at 576 ($T_1$), 665 ($T_2$), and 736 K ($T_3$), whose intensity appears to be independent of the manganese loading. These peaks are interpreted as a stepwise reduction of $MnO_2$ to $Mn_2O_3$, $Mn_2O_3$ to $Mn_3O_4$, and $Mn_3O_4$ to MnO, respectively (Table 2, Fig. 11). In agreement with thermodynamic predictions, further reduction of MnO to metallic manganese does not occur in between 273 and 1073 K [40]. $H_2$-TPR results for nickel-promoted Mn/$TiO_2$ catalysts showed the shift of peak positions to lower temperatures, suggesting that the reduction potential of manganese oxide species is increased compared to those of monometallic catalyst. A two-step reduction profiles (only two peaks) were observed for the Mn–Ni/$TiO_2$ catalysts, whereas three-step reduction profile was observed for

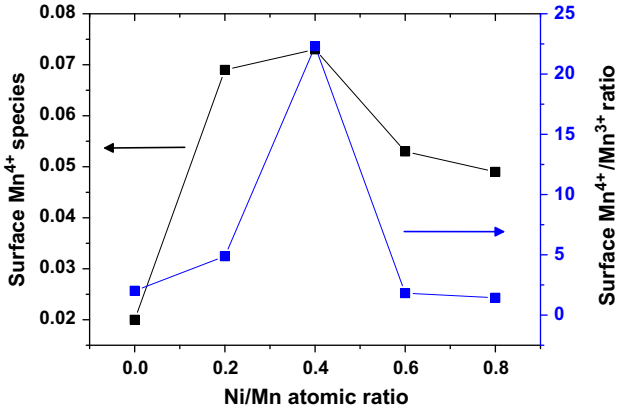


**Fig. 8.** Surface atomic concentration of $Mn^{4+}$ and the surface atomic ratio of $Mn^{4+}/Mn^{3+}$ with respect to the Ni/Mn atomic ratio in the catalyst acquired from the XPS analysis: SCR activity of the particular catalyst is comparable with the surface atomic concentration of $Mn^{4+}$.

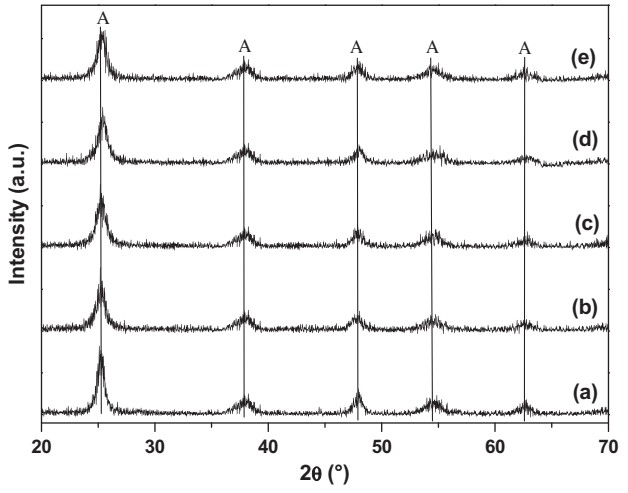


**Fig. 9.** Powder X-ray diffraction patterns of various titania-supported catalysts; according to Ni/Mn atomic ratio (a) $Mn/TiO_2$ (b) $Mn–Ni(0.2)/TiO_2$ (c) $Mn–Ni(0.4)/TiO_2$ (d) $Mn–Ni(0.6)/TiO_2$ and (e) $Mn–Ni(0.8)/TiO_2$, respectively.

$Mn/TiO_2$. The absence of the high-temperature (736 K) peak represents that the dominant phase is $MnO_2$ [41]. Thus, the co-doping of manganese with nickel oxides results in stabilization of the former in the form of $MnO_2$, which is reduced at lower temperatures, compared to $Mn_2O_3$. This raise in reduction potential of manganese and dominant phase of $MnO_2$ seems to be the reason for the increased activity of $Mn–Ni/TiO_2$ catalysts. $H_2$-TPR results are in agreement with the XPS results, where the formation of surface $MnO_2$ phase is increased by the doping of nickel oxide in $Mn/TiO_2$ catalysts.

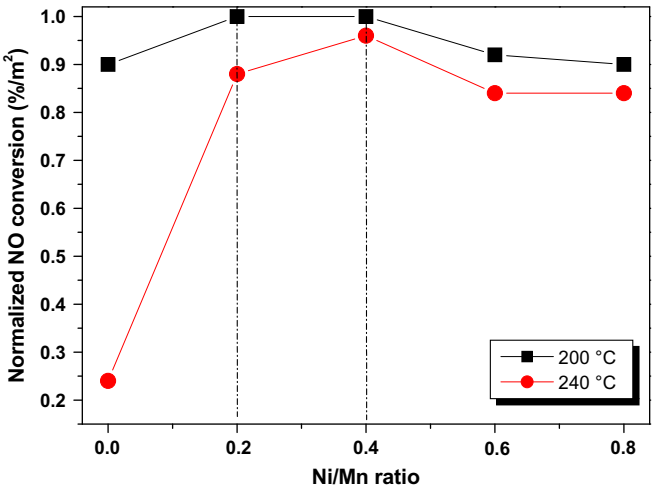


**Fig. 10.** Low-temperature $NH_3$-SCR activity of the $Mn/TiO_2$ and $Mn–Ni/TiO_2$ catalysts normalized by BET surface area. Reaction conditions: NO = 400 ppm, $NH_3$ = 400 ppm, $O_2$ = 2 vol.%, balance He and GHSV = 50,000 $h^{-1}$.

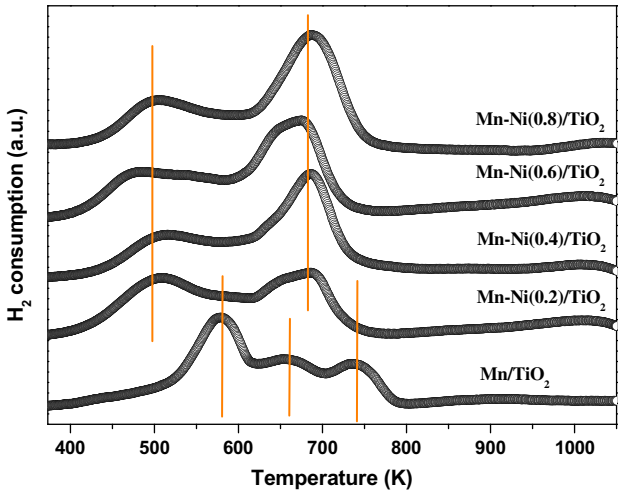


**Fig. 11.** Disappearance of high-temperature peak and low-temperature shift of reduction peaks in $H_2$-TPR patterns of titania-supported manganese–nickel oxide catalysts.

To verify the dispersion of active metal species over the support, the most frequently used and widely accepted method is selective chemisorption of suitable gases like hydrogen and carbon monoxide. Parekh and Weller [42,43] have developed a simple oxygen chemisorption method for determining the dispersion of equivalent metal area over the $Al_2O_3$ support. Consequently, the choice of temperature for the oxygen chemisorption is also crucial. The

**Table 2**
BET surface area and pore volume and $H_2$-TPR measurements.

| Catalyst | XRD phases | $S_{BET}$ ($m^2/g$) | Average pore diameter (nm) | Pore volume ($cm^3/g$) | $T$ (K) | | | $H_2$ consumption (μmol $g^{-1}$) |
|---|---|---|---|---|---|---|---|---|
| | | | | | T-1 | T-2 | T-3 | |
| $TiO_2$ Hombikat (commercial) | A | 309 | 4.5 | 0.37 | – | – | – | – |
| $TiO_2$ Hombikat[b] | A | 161 | 9.3 | 0.42 | – | – | – | – |
| $Mn/TiO_2$ | A | 161 | 9.3 | 0.37 | 576 | 665 | 736 | 282.9 |
| $Mn–Ni(0.2)/TiO_2$[a] | A | 189 | 8.5 | 0.40 | 500 | 689 | – | 335.6 |
| $Mn–Ni(0.4)/TiO_2$[a] | A | 200 | 8.6 | 0.42 | 510 | 684 | – | 339.9 |
| $Mn–Ni(0.6)/TiO_2$[a] | A | 176 | 8.1 | 0.35 | 471 | 673 | – | 352.1 |
| $Mn–Ni(0.8)/TiO_2$[a] | A | 171 | 7.7 | 0.33 | 496 | 685 | – | 398.6 |

[a] Relative amounts are according to the atomic ratio of Ni/Mn; A-anatase;
[b] Calcined at 400 °C.

**Table 3**
Oxygen uptake, active metal dispersion, and STYs of $Mn/TiO_2$ and $Mn–Ni(0.2–0.8)/TiO_2$ catalysts.

| S. no. | Catalyst | $S_{BET}$ ($m^2/g$) | $O_2$ uptake ($\mu mol\ g_{cat}^{-1}$)[a] | Dispersion[b] | NO reaction rate in $\mu mol\ g^{-1}\ s^{-1}$ ($X_{NO}$%)[d] | | STY ($s^{-1}$) at 50,000 GHSV [c] | |
|---|---|---|---|---|---|---|---|---|
| | | | | | 200 °C | 240 °C | 200 °C | 240 °C |
| 1 | $Mn/TiO_2$ | 161 | 215.92 | 0.48 | 08.77 (73.0) | 02.21 (20.0) | 0.49 | 0.12 |
| 2 | $Mn–Ni(0.2)/TiO_2$ | 189 | 238.88 | 0.52 | 11.78 (98.0) | 09.41 (85.0) | 0.61 | 0.49 |
| 3 | $Mn–Ni(0.4)/TiO_2$ | 200 | 245.36 | 0.53 | 12.01 (100) | 10.63 (96.00) | 0.61 | 0.55 |
| 4 | $Mn–Ni(0.6)/TiO_2$ | 176 | 219.84 | 0.48 | 09.73 (81.0) | 08.31 (75.0) | 0.55 | 0.42 |
| 5 | $Mn–Ni(0.8)/TiO_2$ | 171 | 208.06 | 0.45 | 09.25 (77.0) | 07.97 (72.0) | 0.55 | 0.45 |

[a] Pretreatment and $O_2$ pulse chemisorption temperature are 250 °C.
[b] Fraction of manganese atoms at the surface.
[c] Site time yield (STY): number of NO molecules converted per manganese atom site per second.
[d] $X_{NO}$% = NO conversion at corresponding temperature.

pre-reduction temperature must avoid bulk and over reduction of the metal species and sintering of the support material [44]. As shown in our TPR patterns of all catalysts, the first reduction temperature peak appeared around 250 °C related to the reduction of surface interacted support and active bridge (Ti–O–Mn) component, which is very important for the activity of catalyst. For this reason, the pre-reduction temperature of catalysts was selected as 250 °C in favor of the oxygen pulse chemisorption experiments in order to start with the surface reduction of active metal species. In our previous studies, very low SCR activity (5% NO conversion) was observed for the 20 wt.% $Ni/TiO_2$ with 50,000 $h^{-1}$ GHSV at 175 °C suggesting that the nickel is not an active metal for the low-temperature reaction [10]. Hence, in these oxygen chemisorption studies, we have concentrated on the dispersion of active metal species (manganese) over the surface of titania support but not concerning nickel dispersion. In addition, as shown in our TPR patterns, NiO is not supposed to reduce at this pre-reducing temperature. This (single site activity) method is of considerable intrinsic attention as an example of complex reactions operating on single sites (manganese sites). Recently, Zhdanov proposed a kinetic model of standard selective catalytic reduction in NO by $NH_3$ on single sites [45].

The oxygen uptake, active metal dispersion, NO reaction rate, and site time yield (STY) values obtained on various $Mn–Ni/TiO_2$ (Ni/Mn = 0.0–0.8) samples are presented in Table 3. To get insight into the specific activity of the classified Mn species and their relative fraction is combined with the STY values demonstrated in Table 3. As expected, the oxygen chemisorption results indicate that the uptake of $O_2$ per unit weight of catalyst increases with Ni/Mn ratio in the catalyst because of the increased active metal dispersion. The addition of Ni is promoting the dispersion of manganese over the surface of titania support. The oxygen chemisorption and metal dispersion values are increased monotonically up to 0.4 Ni/Mn ratio $Mn–Ni/TiO_2$ catalyst. It becomes virtually high at a loading of Ni/Mn ratio equals to 0.4 in the $Mn–Ni/TiO_2$ catalyst. Further increase in Ni content decreases the oxygen sorption capacity in the catalyst ($Mn–Ni(0.6–0.8)/TiO_2$). This is probably due to the coverage of surface manganese species by approaching high amount of nickel species. This observation is also in agreement with our XPS results, where the ratio of surface active species ($Mn^{4+}$/Ti) decreased behind the 0.4 Ni/Mn ratio.

The acidic sites distribution of the $Mn/TiO_2$ and $Mn–Ni(0.4)/TiO_2$ catalysts was determined using ammonia TPD technique. The similar TPD patterns were observed for the corresponding catalysts (Fig. 12). It is established in the literature that the acid site distribution can broaden by the addition of nickel oxide [46,47]. In the present study, broad acid site distribution is observed for $Mn–Ni(0.4)/TiO_2$ catalyst. It is found in our TPD studies that the doping of nickel can remarkably improve the concentration and acidity of Lewis acid sites on $Mn/TiO_2$ catalyst. Usually, the low-temperature peak is attributed to ammonia coordinated to Lewis acid sites; percentage of this peak area is increased by the addition of nickel with 0.4 Ni/

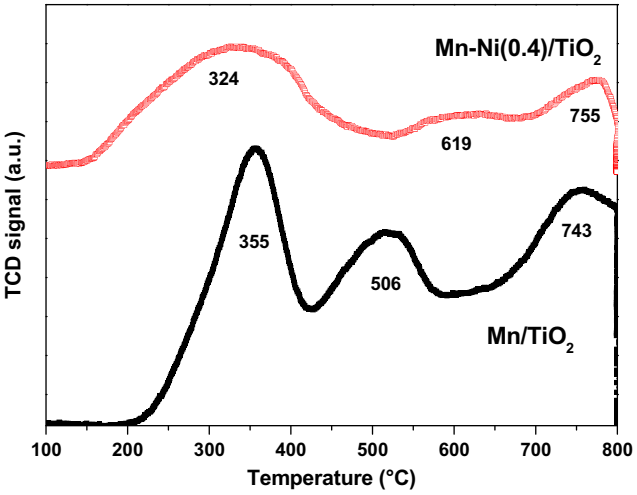


**Fig. 12.** $NH_3$-TPD patterns of $Mn/TiO_2$ and $Mn–Ni(0.4)/TiO_2$ catalysts.

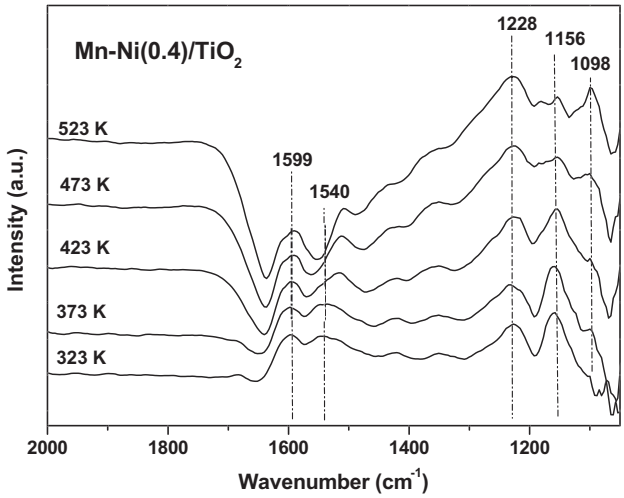


**Fig. 13.** *In situ* FT-IR spectra of adsorbed ammonia species over the $Mn–Ni(0.4)/TiO_2$ catalyst at 323 K and successive outgassing at various temperatures (323–523 K).

Mn atomic ratio. These results are in good agreement with the reported literature, where the doping of nickel can significantly improve the concentration and acidity of Lewis acid sites on $CeO_2$–$ZrO_2$ catalysts [48]. To support this statement, the adsorption and desorption characteristics of $NH_3$ over the $Mn–Ni(0.4)/TiO_2$ catalyst have been investigated to ensure the influence of nickel oxide. *In situ* FTIR experiments were performed in order to gain a better

understanding of molecular behavior of ammonia and to acquire the information about surface species. The adsorption–desorption of ammonia provided information about the nature of acid sites present, and its presence as a function of temperature (323–523 K) revealed the potential strength of the acid sites. In our previous studies, the 1167, 1301, 1467, 1599, and 1680 $cm^{-1}$ peaks are observed for $Mn/TiO_2$ [9] and they correspond to ammonia coordinatively adsorbed on Lewis sites. The *in situ* FTIR spectra of the adsorbed species arising from the interaction of ammonia with the surface of Mn–Ni(0.4)/$TiO_2$ catalyst followed by evacuation at successively increasing temperatures are shown in Fig. 13. The bands at 1098, 1156, and 1228 $cm^{-1}$ peaks were attributed to coordinatively adsorbed $NH_3$ on Lewis sites [48]. Interestingly, an absorption peak at 1156 $cm^{-1}$ ($\delta_s$ $NH_3$ coordinated to Lewis acid sites) decreases down to disappear after evacuation at 473–523 K range. Bands at 1540 and 1599 $cm^{-1}$ are attributed to the $\delta_{as}$ $NH_3$ coordinated to Lewis acid sites [48]. In agreement with the TPD results, we observed similar distinctive *in situ* FTIR spectra for the Mn–Ni(0.4)/$TiO_2$ and $Mn/TiO_2$. The similar features of coordinative adsorbed species (1098, 1156, and 1228 $cm^{-1}$, $\delta_s$ $NH_3$ bound to Lewis acid sites) were observed in both cases. These results suggest that the Mn–Ni(0.4)/$TiO_2$ surface sites are having Lewis acidity, with no apparent Brönsted acidity.

## 4. Conclusions

A series of novel nickel-promoted titania-supported manganese catalysts were prepared by adopting wet impregnation method and developed for the low-temperature selective catalytic reduction (SCR) of NO with ammonia in the presence of oxygen. 100% of NO conversion with 100% $N_2$ selectivity was obtained over the Mn–Ni(0.4)/$TiO_2$ catalyst, at 200 °C, under flow conditions of GHSV = 50,000 $h^{-1}$. It was found from the XRD patterns that the Mn and Ni are highly dispersed over the titania support. Shift in manganese reduction peak (576–510 K) and disappearance of high-temperature peak at 736 K in the TPR profiles suggested that the $MnO_2$ is the dominant phase in Mn–Ni/$TiO_2$ catalysts. Among all the catalysts, deconvoluted XPS spectrum of Mn–Ni(0.4)/$TiO_2$ revealed the high existing amount of $Mn^{4+}$ ions over the surface of titania ($Mn^{4+}$/Ti = 0.073). The Mn–Ni(0.4)/$TiO_2$ catalyst proved its remarkable performance by exhibiting a superior hydrothermal stability with 10 vol.% inlet water concentrations with 240 h on stream. In conclusion, Mn–Ni(0.4)/$TiO_2$ catalyst offers high NO conversion, high $N_2$ selectivity, broadening of temperature window, time on stream patterns, and hydrothermal stability.

## Acknowledgment

The authors wish to acknowledge financial support from the National Science Foundation (Grant No. NSF-0828226).

## References

[1] F. Janssen, F.V. Kerkhof, H. Bosch, J.R.H. Ross, J. Phys. Chem. 91 (1987) 5921.
[2] J.A. Dumesic, N.-Y. Topsoe, H. Topsoe, T. Slabiak, J. Catal. 163 (1996) 409.
[3] G. Busca, L. Lietti, G. Ramis, F. Berti, Appl. Catal. B: Environ. 18 (1998) 1.
[4] H. Tounsi, S. Djemal, C. Petitto, G. Delahay, Appl. Catal. B: Environ. 107 (2011) 158.
[5] J.P. Dunn, P.R. Koppula, H.G. Stenger, I.E. Wachs, Appl. Catal. B: Environ. 19 (1998) 103.
[6] Vanadium Pentoxide, MSDS No. V2220, B. Mallinckrodt, N.J. Phillipsburg, July 1, 2009, <http://www.jtbaker.com/msds/englishhtml/v2220.htm> (accessed 20.01.10).
[7] P.G. Smirniotis, D.A. Peña, B.S. Uphade, Angew. Chem. Int. Ed. 40 (2001) 2479.
[8] D.A. Peña, B.S. Uphade, P.G. Smirniotis, J. Catal. 221 (2004) 421.
[9] D.A. Peña, B.S. Uphade, E.P. Reddy, P.G. Smirniotis, J. Phys. Chem. B 108 (2004) 9927.
[10] E.P. Reddy, E. Neeraja, M. Sergey, P. Boolchand, P.G. Smirniotis, Appl. Catal. B: Environ. 76 (2007) 123.
[11] T. Ishihara, M. Ando, K. Sada, K. Takiishi, K. Yamada, H. Nishiguchi, Y. Takita, J. Catal. 220 (2003) 104.
[12] A.K.H. Nohman, D. Duprez, C. Kappenstein, S.A.A. Mansour, M.I. Zaki, in: B. Delmon, P.A. Jacobs, G. Poncelet (Eds.), Preparation of Catalysts V, Elsevier, Amsterdam, 1991, p. 617.
[13] R. Craciun, B. Nentwick, K. Hadjiivanov, H. Knözinger, Appl. Catal. A 243 (2003) 67.
[14] C. Lahousse, A. Bernier, P. Grange, B. Delmon, P. Papaefthimiou, T. Ioannides, X. Verykiosy, J. Catal. 178 (1998) 214.
[15] C. Reed, Y. Xi, S.T. Oyama, J. Catal. 235 (2005) 378.
[16] Brian R. Strohmeier, David M. Hercules, J. Phys. Chem. 88 (1984) 4922.
[17] P.W. Selwood, T.E. Moore, M. Ellis, K. Wethingt, J. Am. Chem. Soc. 71 (1949) 693.
[18] A.K.H. Nohman, D. Duprez, C. Kappenstein, S.A.A. Mansour, M.I. Zaki, Preparation of catalysts, in: G. Poncelet, P.A. Jacobs, P. Grange, B. Delmon (Eds.), Elsevier, Amsterdam, 1991, p. 617.
[19] M.L. Jacono, M. Schiavello, Preparation of catalysts, in: B. Delmon, P.A. Jacobs, G. Poncelet (Eds.), Elsevier, Amsterdam, 1976, p. 474.
[20] A. Wollner, F. Lange, H. Schmetz, H. Knozinger, Appl. Catal. A 94 (1993) 181.
[21] V.H. Vu, J. Belkouch, A. Ould-Dris, B. Taouk, AIChE J. 54 (2008) 6, doi:10.1002/aic.
[22] Z. Chen, Q. Yang, H. Li, X. Li, L. Wang, S.C. Tsang, J. Catal. 276 (2010) 56.
[23] W.-J. Hong, S. Iwamoto, S. Hosokawa, K. Wada, H. Kanai, M. Inoue, J. Catal. 277 (2011) 208.
[24] W.S. Kijlstra, J.C.M.L. Daamen, J.M. van de Graaf, B. van der Linden, E.K. Poels, A. Bliek, Appl. Catal. B: Environ. 7 (1996) 337.
[25] T. Valdeś-Solıś, G. Marbań, A.B. Fuertes, Appl. Catal. B: Environ. 46 (2003) 261.
[26] X.T. Tang, J.M. Hao, W.G. Xu, J.H. Li, Catal. Commun. 8 (2007) 329.
[27] F. Kapteijn, L. Singoredjo, A. Andreini, Appl. Catal. B 3 (1994) 173.
[28] A.H. Reidies, Manganese Compounds, Ullmann's Encyclopedia of Chemical Technology, Wiley-VCH, Weinheim, 2007, doi:10.1002/14356007.a16_123, <http://en.wikipedia.org/wiki/Manganese(II)_oxide#cite_note-Greenwood-1>.
[29] F.C. Buciuman, F. Patcas, T. Hahn, Chem. Eng. Proc. 38 (1999) 563.
[30] F. Kapteijn, L. Singoredjo, M. Vandriel, A. Andreini, J.A. Moulijn, G. Ramis, G. Busca, J. Catal. 150 (1994) 105.
[31] F. Kapteijn, A.D. van Langeveld, J.A. Moulijn, A. Andreini, M.A. Vuurman, A.M. Turek, J.-M. Jehng, I.E. Wachs, J. Catal. 150 (1994) 94.
[32] A. Machocki, T. Ioannides, B. Stasinska, W. Gac, G. Avgouropoulos, D. Deli2007maris, W. Grzegorczyk, S. Pasieczna, J. Catal. 227 (2004) 282.
[33] S. Ponce, M.A. Pena, J.L.G. Fierro, Appl. Catal. B: Environ. 24 (2000) 193.
[34] J.M.G. Amores, T. Armaroli, G. Ramis, F. Finaochio, G. Busca, Appl. Catal. B: Environ. 22 (1999) 259.
[35] M.R. Morales, B.P. Barbero, L.E. Cadús, Appl. Catal. B: Environ. 67 (2006) 229.
[36] M.R. Morales, B.P. Barbero, L.E. Cadús, Appl. Catal. B: Environ. 74 (2007) 1.
[37] G. Pechi, P. Reyes, T. Lopez, R. Gomez, A. Moreno, J.L.G. Fierro, J. Chem. Technol. Biotechnol. 77 (2002) 944.
[38] M.R. Morales, B.P. Barbero, L.E. Cadús, Fuel 87 (2008) 1177.
[39] M.R. Morales, B.P. Barbero, T. Lopez, A. Moreno, L.E. Cadús, Fuel 88 (2009) 2122.
[40] I.R. Leith, M.G. Howden, Appl. Catal. 37 (1988) 75.
[41] S.M. Saqer, D.I. Kondarides, X.E. Verykios, Appl. Catal. B: Environ. 103 (2011) 275.
[42] B.S. Parekh, S.W. Weller, J. Catal. 47 (1977) 100.
[43] S.W. Weller, Acc. Chem. Res. 16 (1983) 101.
[44] B.M. Reddy, B. Manohar, E.P. Reddy, Langmuir 9 (1993) 1781.
[45] V.P. Zhdanov, React. Kinet. Mech. Cat. 103 (2011) 11.
[46] Z. Si, D. Weng, X. Wu, J. Yang, B. Wang, Catal. Commun. 11 (2010) 1045.
[47] P.M. Sreekanth, P.G. Smirniotis, Catal. Lett. 122 (2008) 37.
[48] J.M.G. Amores, V.S. Escribano, G. Ramis, G. Busca, Appl. Catal. B: Environ. 13 (1997) 45.